Eigenfrequencies of vortex-pair equilibria near an elliptic cylinder or a flat plate in uniform flow

T. W. G. de Laat
Netherlands Defence Academy, P.O. Box 10000, 1780 CA Den Helder, The Netherlands
(Received 23 October 2006; published 2 March 2007)

The eigenfrequencies of the potential-flow equilibria of a symmetric vortex pair behind an elliptic cylinder in uniform flow are calculated through the use of conformal mapping. These frequencies are shown to have values in agreement with measured Strouhal numbers reported in various papers. The special cases of the potential-flow equilibrium of a symmetric vortex pair behind a circular cylinder and the equilibrium behind a flat plate perpendicular to the uniform flow, are related to the measured Strouhal numbers of about 0.21 and 0.15, respectively. It is suggested that in the range of subcritical Reynolds numbers, 3×10^2 to 5×10^5 for the circular cylinder, a part of the drag is the result of the presence of a mean recirculation region in the near wake, which sheds vortices in the far wake and which is fed by vorticity from the cylinder wall.

DOI: 10.1103/PhysRevE.75.036302 PACS number(s): 47.32.cb, 47.15.km, 47.27.wb

I. INTRODUCTION

The presence of vorticity behind a cylinder in uniform flow emerges from the viscosity of the fluid. Although the vorticity is generated by viscous forces, the dynamics of the resulting flowfield with vortices may be governed by inviscid properties of the flow. The mathematical description of the flow can then be given by solutions of Laplace's equation. This inviscid approach gives rise to Föppl's equilibrium for the symmetric vortex pair behind a circular cylinder in uniform flow, e.g., Milne-Thomson [1], p. 370. When symmetrically displaced from that equilibrium, symmetric motion around the equilibrium positions will result. This was reported together with the associated frequencies by de Laat and Coene [2]. Smith [3] has also calculated the eigenvalues in view of a stability analysis.

The unsteadiness behind bluff bodies and especially behind circular cylinders has been measured and reported by many investigators, since it was reported for the first time by Strouhal in 1878 (Roshko [4]). A recent review was made by Sarpkaya [5]. He indicated many unsolved matters and made a large number of recommendations for further experiments to obtain more insight in the parameters of vortex-induced vibrations.

Gerrard [6] suggested with respect to the formation of the vortices behind a circular cylinder that "there is a possible high Reynolds-number flow régime in which the formation region is symmetrical in the absence of free-stream disturbances." Furthermore, Williamson [7] stated, following the results of Roshko [8]: "if one averages over large time (compared to the shedding period) one can define a *mean recirculation region* in the wake, which is symmetric and closed." These observations indicate that symmetric solutions might be relevant for real flow.

In the present paper the eigenfrequencies for an elliptic cylinder or a flat plate with a symmetric vortex pair in uniform flow are calculated through the use of conformal mapping, and evaluated with respect to the unsteadiness found in experiments.

II. EQUILIBRIUM AND FREQUENCY OF MOTION OF A SYMMETRIC VORTEX PAIR BEHIND AN ELLIPTIC CYLINDER IN ONCOMING FLOW

A commonly applied dimensionless number for unsteadiness behind a cylinder is the Strouhal number Sr. This number is related to the frequency f of the oscillations in the flow and the cylinder diameter perpendicular to the uniform flow. For the elliptic cylinder of Fig. 1, with uniform flow U_∞ it is defined as

$$\mathrm{Sr} \equiv \frac{2bf}{U_\infty}. \tag{1}$$

The flowfield in the physical z plane ($z=x+iy$) of Fig. 1 about an ellipse with major axis $2a$ and minor axis $2b$, is obtained through two subsequent transformations as described in Milne-Thomson [1], p. 166, by

$$\zeta = \sigma + \frac{(a+b)^2}{4\sigma} \tag{2}$$

and

$$\sigma = \tfrac{1}{2}(z \pm \sqrt{z^2 - a^2 + b^2}). \tag{3}$$

The flowfield in the ζ plane can be described by the complex potential χ,

$$\chi(\zeta;\zeta_1,\zeta_1^*) = U_\infty\zeta + \frac{i\Gamma}{2\pi}\ln\left(\frac{\zeta-\zeta_1}{\zeta-\zeta_1^*}\right), \tag{4}$$

with ζ_1^* being the complex conjugate of ζ_1.

The vortex velocity follows from Helmholtz's theorem by calculating the local flow velocity. The vortex velocity in the z plane is related to the vortex velocity in the ζ plane. However, the vortex velocity does not simply transform with the conformal mapping. It changes according to the change of the path function described by Routh's correction, see e.g., Lugt [9], p. 162, which in integral form is known as Routh's theorem, e.g., Milne-Thomson [1], p. 372. The velocity of vortex No. 1 in the physical z plane, which we indicate by $V_1 \equiv u_1 + iv_1$, can be calculated using the complex velocity potential in the ζ plane, using Routh's correction by

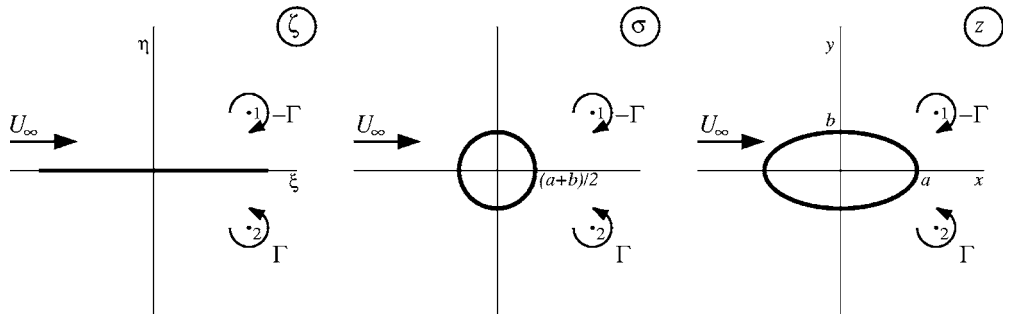

FIG. 1. Transformation of a vortex pair in uniform flow to a vortex pair near a contour, symmetric with respect to the uniform flow.

$$V_1^* \equiv u_1 - iv_1 = \left(\frac{d\chi}{d\zeta} - \frac{i\Gamma}{2\pi}\frac{1}{\zeta - \zeta_1}\right)_{\zeta=\zeta_1} \zeta_1' + \frac{i\Gamma}{4\pi}\left(\frac{\zeta_1''}{\zeta_1'}\right), \quad (5)$$

with $\zeta_1' \equiv (d\zeta/dz)_{z=z_1}$ and $\zeta_1'' \equiv (d^2\zeta/dz^2)_{z=z_1}$. Equilibrium positions (x_0, y_0) are obtained by solving the two equations (real and imaginary part) contained in Eq. (5) for $u_1 - iv_1 = 0$, using (2)–(4), by means of a numerical iteration method. We subsequently take a number of x_0 positions to obtain y_0 and Γ for aspect ratios a/b of 0, 0.5, 1, 1.5, and 2. The equilibrium positions x_0 and y_0 are made dimensionless using b and are plotted in Fig. 2(a). The vortex strength is made dimensionless by

$$G \equiv \frac{\Gamma}{2\pi b U_\infty}, \quad (6)$$

and is plotted against x_0/b in Fig. 2(b).

For $a/b=0$, which yields a flat plate, Smith and Clark [10] reported that it is not possible to have stationary vortices on the leeward side. They gave the proof for the symmetric vortex pair when it satisfies the Kutta condition of smooth flow at the sharp edges of the plate. When this condition is not imposed, equilibrium positions are obtained for the symmetric vortex pair, which are plotted $(a/b=0)$ in Fig. 2(a) with the related vortex strength G in Fig. 2(b).

For $a/b=1$, which yields a circular cylinder, the solution is that of Föppl's equilibrium points, e.g., Milne-Thomson [1], p. 370, which are described by

$$\sin\theta_0 = \frac{1}{2}\left(1 - \frac{b^2}{r_0^2}\right) \quad (7)$$

and

$$G = \frac{r_0}{b}\left(1 - \frac{b^2}{r_0^2}\right)^2\left(1 + \frac{b^2}{r_0^2}\right), \quad (8)$$

with $r_0 = \sqrt{x_0^2 + y_0^2}$ and $\theta_0 = \arctan(y_0/x_0)$. It is easily seen from Eq. (7) that

$$\lim_{r_0\to\infty} \theta_0 = 30°.$$

The equilibria from Eqs. (7) and (8) are plotted in Figs. 2(a) and 2(b), indicated by $a/b=1$. The asymptote is also included in Fig. 2(a).

When a vortex pair in its equilibrium position is given a small disturbance while keeping the vortices symmetric, the vortex-velocity field results in a vortex trajectory around that equilibrium [2]. Substitution of the angular velocity ω, Eq. (13) of Ref. [2] with $f=\omega/(2\pi)$, in (1) yields

$$\mathrm{Sr} = \frac{b^2}{\pi r_0^2}\sqrt{\left(3 - \frac{b^2}{r_0^2}\right)\left(1 + 2\frac{b^2}{r_0^2} + 5\frac{b^4}{r_0^4}\right)}. \quad (9)$$

In Fig. 2(b) the values of the Strouhal number of the eigenfrequency (9) related to the equilibria of (7) and (8) are plotted against x_0/b $(a/b=1)$.

The frequency of the cyclic motion of a vortex around its equilibrium position can also be calculated using a method similar to the procedure used in de Laat and Coene [2],

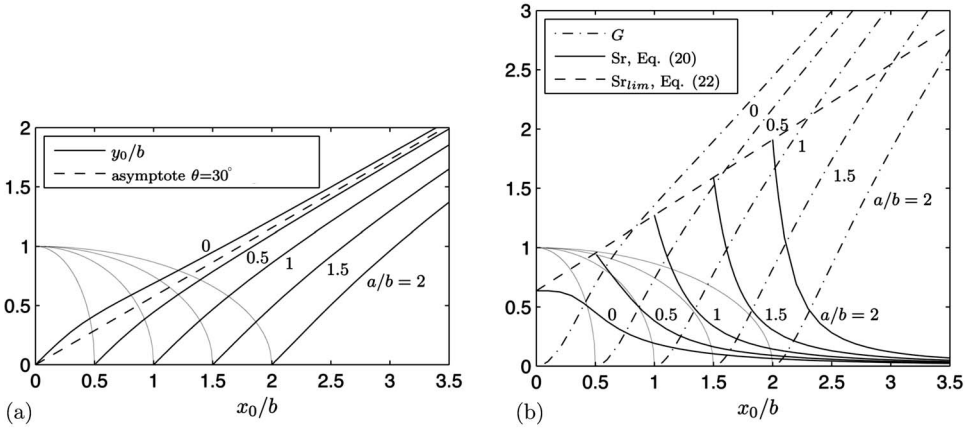

FIG. 2. Equilibrium of a symmetric vortex pair on the leeward side of an ellipse in uniform flow and the related eigenfrequencies. (a) Equilibrium positions; (b) Strouhal number Sr of the eigenfrequency and dimensionless vortex strength G.

which was also used for stability analysis by Smith [3], Huang and Chow [11], Tang and Aubry [12], and Cai *et al.* [13]. It is based on linearization of the vortex velocity near the equilibrium position and omitting second-order and higher-order terms. We substitute $z_1=z_0+\Delta z_1$ combined with (2)–(4), in vortex velocity Eq. (5), with z_0 being the equilibrium position and $\Delta z_1=\Delta x_1+i\Delta y_1$ a small displacement. We use the following formulation:

$$\begin{bmatrix} u_1 \\ v_1 \end{bmatrix} = \begin{bmatrix} \left(\frac{\partial u_1}{\partial x_1}\right)_{z_1=z_0} & \left(\frac{\partial u_1}{\partial y_1}\right)_{z_1=z_0} \\ \left(\frac{\partial v_1}{\partial x_1}\right)_{z_1=z_0} & \left(\frac{\partial v_1}{\partial y_1}\right)_{z_1=z_0} \end{bmatrix} \begin{bmatrix} \Delta x_1 \\ \Delta y_1 \end{bmatrix} + O(\Delta z_1^2).$$

This system of two first-order differential equations for the perturbation $(\Delta x_1, \Delta y_1)$, can be solved using the method of eigenvalues. The eigenvalues λ of this linearized system are for $z_1=z_0$,

$$\lambda_{1,2} = \left[\frac{1}{2}\left(\frac{\partial u_1}{\partial x_1} + \frac{\partial v_1}{\partial y_1}\right) \pm \sqrt{\frac{1}{4}\left(\frac{\partial u_1}{\partial x_1} + \frac{\partial v_1}{\partial y_1}\right)^2 - \left(\frac{\partial u_1}{\partial x_1}\frac{\partial v_1}{\partial y_1} - \frac{\partial v_1}{\partial x_1}\frac{\partial u_1}{\partial y_1}\right)} \right]_{z_1=z_0}. \tag{10}$$

The equilibrium is stable when the real parts of both eigenvalues are negative, implying that if the equilibrium is disturbed with $(\Delta x_1, \Delta y_1)$, the displacement will tend to zero. From Eq. (5) we determine the derivatives required in (10) using

$$u_1 = (V_1 + V_1^*)/2, \tag{11}$$

$$v_1 = (V_1 - V_1^*)/(2i), \tag{12}$$

and $z_1=x_1+iy_1$. It follows that

$$\frac{\partial u_1}{\partial x_1} = \frac{1}{2}\left(\frac{\partial (V_1 + V_1^*)}{\partial z_1} + \frac{\partial (V_1 + V_1^*)}{\partial z_1^*}\right), \tag{13}$$

$$\frac{\partial u_1}{\partial y_1} = i\frac{1}{2}\left(\frac{\partial (V_1 + V_1^*)}{\partial z_1} - \frac{\partial (V_1 + V_1^*)}{\partial z_1^*}\right), \tag{14}$$

$$\frac{\partial v_1}{\partial x_1} = -i\frac{1}{2}\left(\frac{\partial (V_1 - V_1^*)}{\partial z_1} + \frac{\partial (V_1 - V_1^*)}{\partial z_1^*}\right), \tag{15}$$

$$\frac{\partial v_1}{\partial y_1} = \frac{1}{2}\left(\frac{\partial (V_1 - V_1^*)}{\partial z_1} - \frac{\partial (V_1 - V_1^*)}{\partial z_1^*}\right). \tag{16}$$

Substitution of (5) combined with flowfield (4) and transformation $\zeta(z)$ through combination of (2) and (3) into (13) and (16) yields

$$\frac{\partial u_1}{\partial x_1} + \frac{\partial v_1}{\partial y_1} = 0. \tag{17}$$

Furthermore we obtain after substitution of Eqs. (13)–(17) into the eigenvalues (10),

$$\lambda_{1,2} = \pm \sqrt{-\left(\frac{\partial V_1}{\partial z_1}\frac{\partial V_1^*}{\partial z_1^*} - \frac{\partial V_1^*}{\partial z_1}\frac{\partial V_1}{\partial z_1^*}\right)}. \tag{18}$$

For the equilibria treated in this paper it was found that all eigenvalues are imaginary, so the equilibrium is neutrally stable in these cases and the vortices will move around their equilibrium positions in the same way as described in de Laat and Coene [2] for the case of the symmetric vortex pair near the circular cylinder in uniform flow or the single vortex in a corner stagnation flow. The angular velocity of this motion now follows from (18):

$$\omega = \sqrt{\frac{\partial V_1}{\partial z_1}\frac{\partial V_1^*}{\partial z_1^*} - \frac{\partial V_1^*}{\partial z_1}\frac{\partial V_1}{\partial z_1^*}} \quad \text{(rad/s)}. \tag{19}$$

With the definition of the Strouhal number (1), we have with frequency $f=\omega/(2\pi)$ in s^{-1},

$$\mathrm{Sr} = \frac{b}{\pi U_\infty}\sqrt{\frac{\partial V_1}{\partial z_1}\frac{\partial V_1^*}{\partial z_1^*} - \frac{\partial V_1^*}{\partial z_1}\frac{\partial V_1}{\partial z_1^*}}. \tag{20}$$

The Strouhal numbers of the motion around the equilibrium points of Fig. 2(a) are calculated using Eq. (20) and included in Fig. 2(b). For $a/b=1$ the curve is identical to that of Eq. (9).

The limiting Strouhal number for the equilibrium approaching the rear stagnation point $(a,0)$, so for $\Gamma \to 0$, can be found by a local approximation of the flowfield near that stagnation point. From the flowfield represented by (4) with the transformation $\zeta(z)$ from (2) and (3) we find after substitution of $z=a+\varepsilon$ with $\varepsilon \ll a$, for the flow velocity near the stagnation point to first order,

$$u - iv = U_\infty \frac{a+b}{b^2}\varepsilon. \tag{21}$$

With Eq. (5) from de Laat and Coene [2] we have that the angular velocity of a vortex about its equilibrium position in a corner stagnation flowfield has the value $\omega=2k$, with k the proportional factor of the stagnation flow. From (21) we now have $k=U_\infty(a+b)/b^2$ so $\omega=2U_\infty(a+b)/b^2$. With the definition of the Strouhal number (1) and $f=\omega/(2\pi)$ we find

$$\lim_{r_0 \to a} \mathrm{Sr} = \frac{2}{\pi}\left(1 + \frac{a}{b}\right). \tag{22}$$

Substitution of a/b equal to 0, 0.5, 1, 1.5, and 2, yields the limiting values of the Strouhal number of, respectively, $\mathrm{Sr}=2/\pi \approx 0.637$, $\mathrm{Sr}=3/\pi \approx 0.955$, $\mathrm{Sr}=4/\pi \approx 1.273$ [which is also found when applying Eq. (9)], $\mathrm{Sr}=5/\pi \approx 1.592$, and $\mathrm{Sr}=6/\pi \approx 1.910$. Equation (22) is plotted in Fig. 2(b) and the limiting values are included in Table I.

III. COMPARISON WITH EXPERIMENTAL DATA

Unsteadiness of vortex flows has been reported on many occasions, especially for the flow past a circular cylinder $(a/b=1)$. Experimental results were found in various sources for values of a/b of 0, 0.5, 1, and 2. In this section these experimental results are compared with the values calculated

TABLE I. Vortex-pair equilibria and measured values of Sr and G.

Point-vortices equilibrium						Measured values		
a/b	x_0/b	y_0/b	G	Sr	Remark	Sr	$\mathrm{Re}/10^4$	Source
0	0	0	0	0.637	$\mathrm{Sr}=2/\pi$			
0	1.131	0.756	1.501	0.161	Sr=0.161	0.161	0.4	Abernathy [14]
0	1.186	0.785	1.560	0.150	Sr=0.150			
0	1.208	0.796	1.584	0.146	Sr=0.146	0.146	3–19	Fage and Johansen [15]
0	1.272	0.829	1.652	0.135	Sr=0.135	0.135	0.3–1.7	Roshko [16]
0.5	0.5	0	0	0.955	$\mathrm{Sr}=3/\pi$			
0.5	1.380	0.708	1.348	0.195	Sr=0.195	0.195	11-60	Delany and Sorensen [17]
1	1	0	0	1.273	$\mathrm{Sr}=4/\pi$			
1	1.364	0.348	0.519	0.460	Sr=0.460	0.46	55	Bearman [18]
1	1.392	0.373	0.574	0.430	Sr=0.430	0.43	12	Delany and Sorensen [17]
1	1.499	0.467	0.780	0.337	$G=0.780$		0.0062	Schaefer and Eskinazi [19], $G\approx 0.78$
1	1.531	0.494	0.840	0.316	$G=0.840$		0.0080	Green and Gerrard [20], $G\approx 0.84$
1	1.680	0.615	1.110	0.237	$G=1.110$		0.0102	Green and Gerrard [20], $G\approx 1.11$
1	1.722	0.649	1.184	0.220	Sr=0.220	0.22	3–7	Sarioglu and Yavuz [21]
1	1.750	0.670	1.231	0.210	Sr=0.210			
1	1.779	0.693	1.281	0.200	Sr=0.200	0.20	0.01–1.7	Roshko [16], Table I, averaged
1	2.141	0.960	1.857	0.120	Sr=0.120	0.12	0.0050	Roshko [4]
1.5	1.5	0	0	1.592	$\mathrm{Sr}=5/\pi$	No measurements found		
2	2	0	0	1.910	$\mathrm{Sr}=6/\pi$			
2	2.238	0.242	0.322	0.600	Sr=0.600	0.60	110–200	Delany and Sorensen [17]
2	2.995	0.958	1.814	0.120	Sr=0.120	0.12	35–50	Delany and Sorensen [17]

with the expressions produced in the preceding section. The experimental results are listed in Table I in advancing order of G, together with some calculated values. The column "Remark" displays the condition for which the equilibrium at that row has been calculated. The Reynolds number Re is related to the width $2b$ of the cylinder perpendicular to the uniform flow, so

$$\mathrm{Re} \equiv \frac{U_\infty 2b}{\nu}, \tag{23}$$

with ν the kinematic viscosity of the fluid.

A. $a/b=0$, flat plate

Experiments with a flat plate in a uniform flow were made by Fage and Johansen [15], Roshko [16], and Abernathy [14]. Fage and Johansen [15] measured a frequency which had a Strouhal number related to the span of 0.146, which is included in Table I. The Reynolds number was estimated by the present author, using kinematic viscosity $\nu=1.45\times10^{-5}$ m^2/s of air at 15 °C. Roshko [16] measured a range of Strouhal numbers of 0.132 to 0.140 in the range of Reynolds numbers between 3020 to 10 600 (his Table I), the average of 0.135 is included in Table I. Abernathy [14] measured Strouhal numbers of 0.161 to 0.244, with increasing blockage factor of the wind tunnel. The value of the least blockage Sr=0.161 is included in Table I, also with an estimated Reynolds number as described above.

If we assume the mean measured Strouhal number of 0.15, we can calculate the equilibrium with the method described in the preceding section and we find the equilibrium of $G=1.560$ at $x_0/b=1.186$ and $y_0/b=0.785$. In Fig. 3 streamlines are plotted for this equilibrium at Sr=0.15. It is to be seen in this figure that this case approximates the case that the Kutta condition of smooth flow at the sharp edge is fulfilled. Smith and Clark [10] have clearly shown that for the inviscid case there is no equilibrium position at which the Kutta condition is satisfied. The locus of solutions for the zero vortex velocity, that we have calculated and plotted in Fig. 2(a) for $a/b=0$ is very near the locus of solutions for the smooth-flow condition at the sharp edge. The equilibrium at Sr=0.15 nearly fulfills the condition of smooth flow at the sharp edges, as shown in Fig. 3. It seems likely that in real flow the viscous effect at the tip smoothens the difference at the sharp edge between this vortex-pair equilibrium solution (zero vortex velocity) and the solution of exact smooth flow at the edge, which for the same vortex strength lies very near the zero vortex velocity solution.

B. $a/b=0.5$

Experimental data for the elliptic cylinder with $a/b=0.5$ is reported by Delany and Sorensen [17]. They measured

$\mathrm{Sr} \approx 0.19-0.20$ in the range $1.1\times10^5 < \mathrm{Re} < 6\times10^5$, the average value of Sr=0.195 is included in Table I. The measured Strouhal number is higher than those of the flat plate, which is in accordance with the predicted tendency with varying a/b as shown in Fig. 2(b).

C. $a/b=1$, circular cylinder

Many experiments have been performed on the flowfield of the circular cylinder in uniform flow since Strouhal reported the unsteadiness for the first time in 1878 (Roshko [4]). Vortex shedding and the formation of a Kármán vortex street are known to be a mechanism of unsteadiness. In this section it is shown that the Strouhal numbers of the eigenfrequencies of the motion around the equilibria of the preceding section and the related vortex strengths, are in agreement with the measured values of the real flow at Reynolds numbers higher than approximately 300 and may be a driving factor in the shedding frequency.

Some results of measured unsteadiness or measured vortex strength are again listed in Table I. In addition to the measured values, the related values of x_0/b, G or Sr are calculated with (8) and (9), respectively [(5) and (20) give the same results] and are added to the table. The corresponding equilibrium points can be found on the curves in Fig. 2. The measurements are evaluated below in three ranges of Reynolds numbers, respectively, $0<\mathrm{Re}<40$, $40<\mathrm{Re}<300$, and $\mathrm{Re}>300$.

1. 0<Re<40

In this range of Reynolds numbers two distinct vortices become clearly visible when injecting particles in the flow, as shown in Fig. 4(a). The flow can be compared with the potential flowfield of Fig. 1 with complex potential (4) and transformation (2).

Although the Strouhal number of the eigenfrequency of the equivalent equilibria can be calculated, there is no unsteadiness reported in this range of Reynolds numbers. This may be due to the dominance of the viscous forces, which dampens the inviscid motion. For the flowfield of Fig. 4(a) the Reynolds number is not known [22] but the flow matches quite well that of Fig. 4(b), although there is the difference of a small secondary vortex. The closed-flow region of Fig. 4(a) is not as wide as in the inviscid flow of Fig. 4(b) but the end of the recirculation region, the free stagnation point, correlates well. In real flow, of course, not all of the vorticity is concentrated in one point as it is in the case of the potential-flow model.

2. 40<Re<300

In the range of Reynolds numbers of $40<\mathrm{Re}<150$ a stable Kármán vortex street is known to be formed. For $150<\mathrm{Re}<300$ Roshko [4] reported that an irregular flowfield is being formed. He found from wind tunnel measurements that the unsteadiness started at about Re=40. From Re=50 to 150 the Strouhal number continuously rises to 0.18, with relation

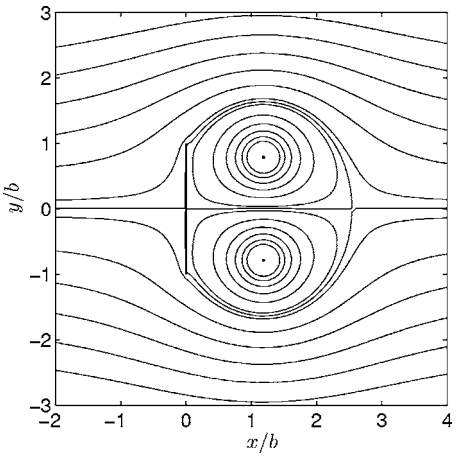

FIG. 3. Streamlines of the flowfield of a vortex pair behind a flat plate ($a/b=0$) for $G=1.560$, Sr=0.150.

$$\mathrm{Sr} \approx 0.212\left(1-\frac{21.2}{\mathrm{Re}}\right), \tag{24}$$

which is represented by the rising part for $\mathrm{Re}<150$ of the Strouhal curve in Fig. 5. Substitution of Re=50 into (24) from Roshko's experimental data yields Sr=0.12. This Strouhal number corresponds to the eigenfrequency of the equilibrium at $G=1.86$, see Fig. 4(d).

For the flow of water Green and Gerrard [20] obtained from experiment that at Re=80 (their Fig. 13) vortices are shed from the circular cylinder with a dimensionless strength $G=0.84$, which corresponds to an equilibrium position from (8) with a Strouhal number of its eigenfrequency (9) of 0.32, see Table I. They did not measure the Strouhal number. Roshko found in wind tunnel measurements a Strouhal number of 0.16, which follows upon substitution of Re=80 into (24). From (8) it then follows that $G=1.55$, which is larger than the maximum value found in the results from measurements listed in Table I. There is quite a difference in the eigenfrequency of the equilibrium at that vortex strength and the Strouhal number measured by Roshko.

Schaefer and Eskinazi [19] measured a vortex strength with dimensionless value $G=0.78$ at Re=62, see Table I.

Green and Gerrard [20] furthermore measured the vortex strength up to Re=102. The dimensionless vortex strength G appeared to increase linearly in this range to $G=1.11$ (their Fig. 16). This maximum dimensionless vortex strength of $G=1.11$ at Re=102, would correspond to Föppl's equilibrium position (8) with a Strouhal number of its eigenfrequency (9) of Sr=0.24, see Table I. From the measurements of Roshko we have at Re=102 through Eq. (24): Sr=0.17, so there is still some difference. The measured increase in vortex strength with increasing Reynolds number would for Föppl's equilibrium relate to an increase in r_0/b from (8) and thus a decrease in Strouhal number from the symmetric eigenfrequency (9). This is clearly not the case as follows from Eq. (24), see also Fig. 5, so the oscillation in the range $\mathrm{Re}<300$ appears not related to the eigenfrequency of Föppl's equilibrium positions.

3. Re>300

From Fig. 5 it is noted that in the range for $\mathrm{Re}=3\times10^2$ up to $\mathrm{Re}=5\times10^5$ the Strouhal number varies between 0.2–0.22.

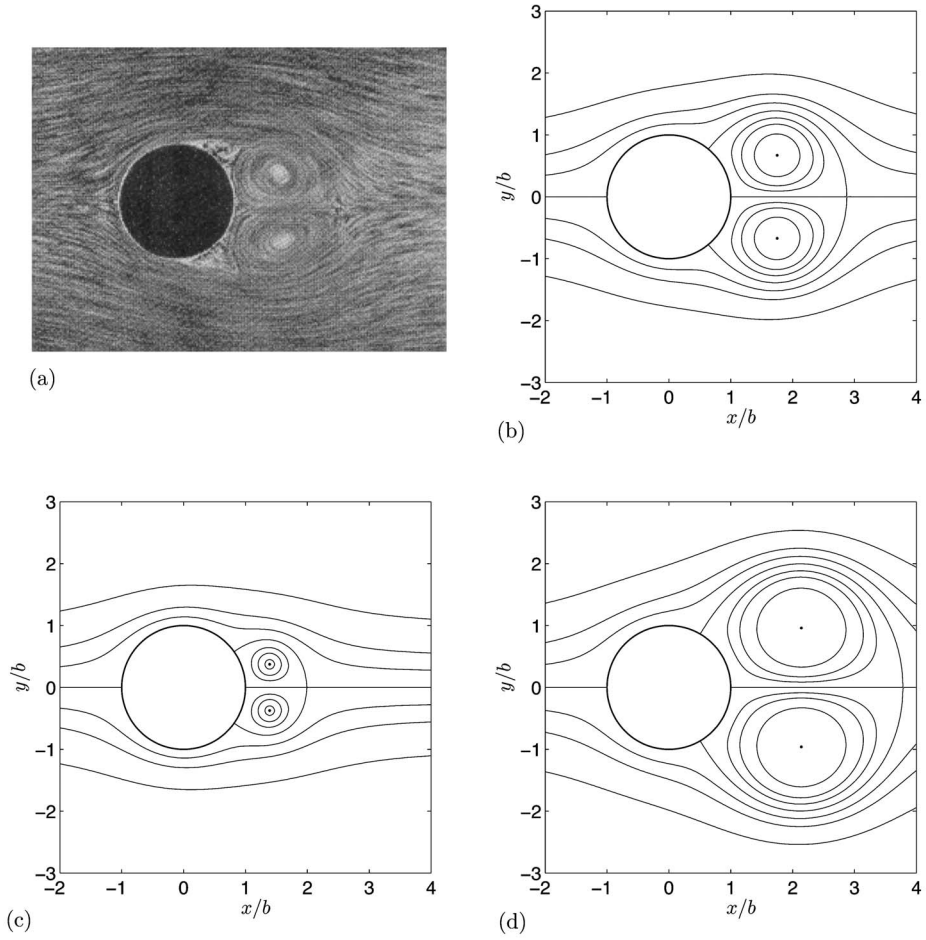

FIG. 4. Streamlines of the flowfield of a vortex pair behind a circular cylinder ($a/b=1$). (a) Streamlines at unknown Re, from Prandtl and Tietjens [22], p. 279; (b) $G=1.231$, Sr=0.210; (c) $G=0.574$, Sr=0.430; (d) $G=1.857$, Sr=0.120.

These values consistently appear in many measurement reports. Sarioglu and Yavuz [21] measured a Strouhal number of about 0.22 in the range $3\times10^4<\mathrm{Re}<7\times10^4$, see Table I. They produced an overview in their Fig. 19 with measurements from others in the range $2\times10^4<\mathrm{Re}<2.5\times10^5$ with Strouhal numbers between 0.19 and 0.22, and a measured Strouhal number of 0.24 at $\mathrm{Re}=2\times10^4$. From (9) and (8) we find that a Strouhal number of 0.21 corresponds to the equilibrium point at $G=1.231$ (see Table I). The flowfield of the vortex pair at this equilibrium position, produced with the velocity potential, is shown in Fig. 4(b) and is quite realistic.

Bloor and Gerrard [24] measured the dimensionless vortex strength of the shed vortices at a large distance (12 times the cylinder radius), which had a strength of $G\approx0.5$ in the range $1\times10^3<\mathrm{Re}<1\times10^4$. This result is not listed in Table I, as at this large distance attenuation of the vortex strength is to be expected. It is indicative for the vortex strength, though, and it is a confirmation that the calculated values of the dimensionless vortex strength are realistic.

A Strouhal number of 0.46 was measured by Bearman [18] at about $\mathrm{Re}=5.5\times10^5$. He observed: "when the time-mean drag coefficient is a minimum the Strouhal number has a maximum value of 0.46." The eigenfrequency with Sr =0.46 corresponds in the present model to a decreased amount of vorticity present in the wake at a dimensionless circulation $G=0.52$.

At Reynolds numbers related to the transition of laminar to turbulent flow upstream of the separation point of the boundary layer, which results in a narrower wake and a lower pressure drag and consequently the well-known decrease of drag coefficient C_D, a rise in Strouhal number from Sr=0.2 at $\mathrm{Re}=3\times10^5$ to Sr=0.43 at $\mathrm{Re}=1.5\times10^6$ is observed, as shown in Fig. 5. An increase in eigenfrequency in the present model corresponds to a decrease in circulation or vortex strength, for instance Strouhal number Sr=0.43 corresponds to $G=0.57$ in comparison with Sr=0.21 at $G=1.23$. These flowfields are shown, respectively, in Figs. 4(c) and 4(b). This would strongly suggest that a portion of the drag of the cylinder in the range $3\times10^2<\mathrm{Re}<5\times10^5$ is related to the vorticity present on the leeward side of the cylinder. Furthermore it is noted from Fig. 5 that the tendency of the C_D to decrease in the range of Reynolds numbers from 0.1 to 1×10^3, changes to about a constant C_D in the range $1\times10^3<\mathrm{Re}<5\times10^5$. The extra drag which is indicated by the present author as a hatched area in Fig. 5, might be due to an amount of vorticity present behind the cylinder, with a circulation of $G\approx1.23$, which would also be accountable for the Strouhal number of 0.21 in that range.

These findings may be explained by the reasoning, which now follows. The vorticity being shed from the cylinder wall can stay in the near wake under influence of the interaction of the vortex with the wall. This interaction with the cylinder

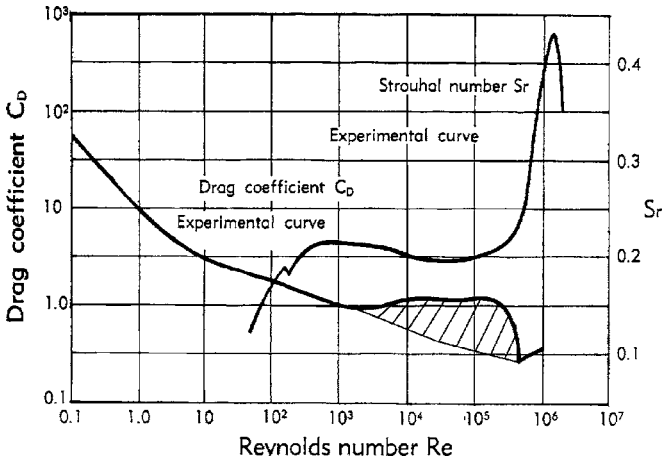

FIG. 5. Variation of Strouhal number and drag coefficient with Reynolds number for the flow over a circular cylinder, from Lagerstrom [23], with region of "vortex drag" (hatched area) indicated by the present author.

wall is a basic mechanism in the oscillatory motion of the vortex about its equilibrium, see Ref. [2]. The vorticity from the two sides of the cylinder form two vortices with opposite sign which can reside without velocity in Föppl's equilibrium positions. The vortices in these equilibrium positions are, however, easily shed into the far wake upon asymmetrical disturbances of the flow (this asymmetry may be in vortex position or strength, see de Laat and Coene [2]). Vorticity is, however, also continuously being shed from the wall into the near wake, thus forming new vortices. So vortices can continuously being shed into the far wake while still maintaining two vortices in the near wake, as suggested by Williamson [7]: "if one averages over large time (compared to the shedding period), one can define a *mean recirculation region* in the wake, which is symmetric and closed."

The critical Reynolds number for the C_D drop, is known to be triggered by the onset of turbulence in the boundary layer, with consequently a higher level of disturbances in the downstream flow. This could well cause the vortices being more easily shed into the far wake, as a vortex is then more easily disturbed from its equilibrium which is unstable for asymmetric disturbances [2], whereas the feeding of vorticity from the cylinder wall is not proportionally increased at the higher flow velocity. The mean recirculation region can then be modeled by a vortex pair with lower strength, which has a higher eigenfrequency of the symmetric motion, compared to the subcritical vortex pair.

The force due to a symmetric vortex pair near the circular cylinder is elaborated upon in de Laat and Coene [25], a contour plot of the dimensionless force per unit depth $F_x/(\rho U_\infty{}^2 b)$ from that study is reproduced in Fig. 6. The negative-force regions are indicated in gray. This force has a maximum for the limit when the vortex pair would approach the inviscid-flow separation point $(a/b,0)$ on the outer side of Föppl's equilibrium curve, which is also the zero-force curve *independent of the vortex strength* as shown in de Laat and Coene [25]. When a vortex pair would move inviscidly around its equilibrium without any disturbances the mean time-dependent force on the cylinder would be zero. When

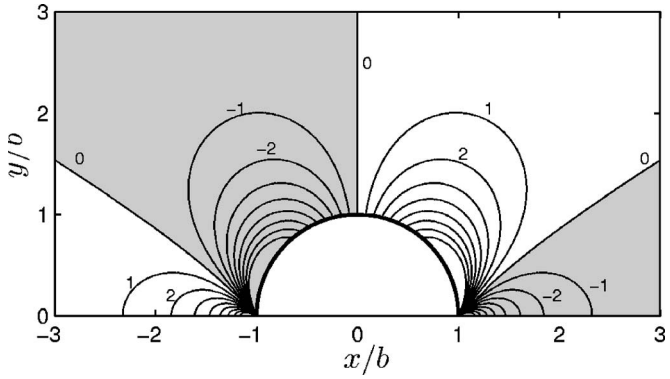

FIG. 6. Dimensionless force on the circular cylinder $F_x/(\rho U_\infty{}^2 b)$, with increments of 1, by the symmetric vortex pair as function of position of vortex 1 for $G=1$, from de Laat and Coene [25].

the vortex pair is intended to model a mean recirculation region, it might however, have a mean position which is not at the equilibrium position, where it would yield zero force on the cylinder in agreement with d'Alemberts paradox applicable for steady flow. Displaced from that equilibrium the vortices have a nonzero velocity and the flow will be unsteady and yield a time-dependent force on the cylinder.

The position of the vortex pair representing the mean recirculation region can be estimated by the trajectory of the shed vortices and the distribution of the feeding vorticity. The exact calculation would require a more detailed model of the equations of motion of the fluid. It can, however, be argued that the position of the mean recirculation region would be on the outer side of the equilibrium curve. The motion of a vortex around its equilibrium is in the direction of the outer flow on the far side of the equilibrium position from the axis of symmetry (x axis), and the vortex velocity is in the opposite direction near the axis of symmetry. So when symmetrically disturbed from their equilibrium positions the vortices will rotate around their equilibrium positions in the same direction as their direction of circulation. Upon disturbance from the equilibrium toward the axis of symmetry the vortex would thus move toward the cylinder and while approaching the cylinder it would move to the outside before being shed into the far wake, whereas upon being displaced from the equilibrium away from the axis of symmetry it would directly be shed into the far wake without traveling around the equilibrium position through the region between equilibrium position and x axis. As the vortices would be randomly disturbed, the shed vortices would spend more time on the far side of the equilibrium point from the axis of symmetry, and consequently the mean center of circulation would also be further to that far side. Moreover as the vorticity is shed from the wall its mean center will also be on the outside of the zero-force curve. The vortex pair which is intended to model the mean recirculation region would thus reside in the area with positive force, outside the zero-force curve, see Fig. 6 and could consequently account for a part of the drag force ("vortex drag") such as indicated by the hatched area in Fig. 5.

D. $a/b=2$

Experimental data for the elliptic cylinder with $a/b=2$ is reported by Delany and Johansen [17]. They measured Sr

≈ 0.12 for $\mathrm{Re}=3.5\times10^5$ and 5×10^5, and $\mathrm{Sr}\approx0.60$ in the range $1.1\times10^6<\mathrm{Re}<2\times10^6$. We thus have a similar transition as with the circular cylinder, though, the subcritical Strouhal number is lower (0.12 compared with 0.22), whereas the supercritical Strouhal number is higher (0.6 compared with 0.46). This higher supercritical Strouhal number is in agreement with the higher predicted value near the stagnation point, see Fig. 2(b). The lower subcritical Strouhal number would imply more vorticity being present behind the elongated ellipse compared to the circular cylinder.

IV. CONCLUSIONS

The relatively simple potential-flow eigenfrequencies of the equilibria of a symmetric vortex pair near an elliptic cylinder in uniform flow are calculated using conformal mapping.

Equilibrium positions and eigenfrequencies for a flat plate perpendicular to the uniform flow ($a/b=0$) with a symmetric vortex pair are obtained, without Kutta condition for smooth flow at the edges. When disturbed from its equilibrium position the symmetric vortex pair will move around this position with an eigenfrequency, which is in agreement with measured Strouhal numbers reported by various papers. The equilibrium flowfield related to the eigenfrequency with Strouhal number 0.15, which is often measured, approximates indeed the flowfield of a flat plate perpendicular to the uniform flow with a symmetric vortex pair, apart from a small difference from smooth flow at the sharp edges of the plate, which could be smoothened by viscosity in a real flow.

Comparison of the eigenfrequencies of the vortex-pair equilibria of a circular cylinder in uniform flow with measured Strouhal numbers reported elsewhere, showed that the measured frequencies agree with these eigenfrequencies, especially for the Strouhal number of about 0.21 for Reynolds numbers between 3×10^2 and 5×10^5. So, although viscosity determines the amount of vorticity that is being shed into the wake of the cylinder, the resulting unsteadiness in the flow is in agreement with the symmetric potential-flow approximation.

It is suggested that for the circular cylinder in the range of Reynolds numbers $3\times10^2<\mathrm{Re}<5\times10^5$ a part of the drag is the result of the presence of a mean recirculation region in the near wake of the circular cylinder as proposed by Williamson [7], which sheds vortices into the far wake and which is fed by vorticity from the cylinder wall. This recirculation region could be modeled by a vortex pair, the mean position of which would be on the outside of the zero-force curve yielding "vortex drag." This mechanism would be expected to be generally applicable to bluff cylinders.

For the elliptic cylinder with $a/b=2$ the same rise in Strouhal number associated with a decreased recirculation region and decreased C_D was observed by Delany and Sorensen [17]. This rise in Strouhal number with decreased vortex strength is in agreement with calculated values of the inviscid point-vortex model.

It is concluded that the relatively simple inviscid motion of a symmetric vortex pair near its equilibrium position may play an important role in the unsteadiness behind bluff bodies as shown for the elliptic cylinders and the flat plate.

ACKNOWLEDGMENTS

The author is grateful to H. W. M. Hoeijmakers of the University of Twente, the Netherlands, for many fruitful discussions on this subject and to a referee, who's comment brought about an improvement in clarity of the discussion on the suggested "vortex drag."

[1] L. M. Milne-Thomson, *Theoretical Hydrodynamics*, 5th ed. (Dover, New York, 1967).
[2] T. W. G. de Laat and R. Coene, J. Fluid Mech. **305**, 93 (1995).
[3] A. C. Smith, J. Appl. Mech. **40**, 610 (1973).
[4] A. Roshko, NACA Report No. 1191, supersedes NACA TN 2913.
[5] T. Sarpkaya, J. Fluids Struct. **19**, 389 (2004).
[6] J. H. Gerrard, J. Fluid Mech. **25**, 401 (1966).
[7] C. H. K. Williamson, Annu. Rev. Fluid Mech. **28**, 477 (1996).
[8] A. Roshko, J. Wind. Eng. Ind. Aerodyn. **49**, 79 (1993).
[9] H. J. Lugt, *Introduction to Vortex Theory* (Vortex Flow Press, Potomac, Maryland, 1996).
[10] J. H. B. Smith and R. W. Clark, AIAA J. **13**, 1114 (1975).
[11] M. K. Huang and C. Y. Chow, AIAA J. **34**, 1182 (1996).
[12] S. Tang and N. Aubry, Phys. Fluids **9**, 2550 (1997).
[13] J. Cai, F. Liu, and S. Luo, J. Fluid Mech. **480**, 65 (2003).
[14] F. H. Abernathy, J. Basic Eng. **84**, 380 (1962).
[15] A. Fage and F. C. Johansen, Proc. R. Soc. London, Ser. A **116**, 170 (1927).
[16] A. Roshko, NACA Technical Note 3169.
[17] N. K. Delany and N. E. Sorensen, NACA Technical Note 3038.
[18] P. W. Bearman, J. Fluid Mech. **37**, 577 (1969).
[19] J. W. Schaefer and S. Eskinazi, J. Fluid Mech. **6**, 241 (1959).
[20] R. B. Green and J. H. Gerrard, J. Fluid Mech. **226**, 219 (1991).
[21] M. Sarioglu and T. Yavuz, AIAA J. **40**, 1257 (2002).
[22] L. Prandtl and O. G. Tietjens, *Applied Hydro- and Aeromechanics* (Dover, New York, 1957).
[23] P. A. Lagerstrom, *Laminar Flow Theory* (Princeton University Press, Princeton, NJ, 1996).
[24] M. S. Bloor and J. H. Gerrard, Proc. R. Soc. London, Ser. A **294**, 1438 (1966).
[25] T. W. G. de Laat and R. Coene, AIAA J. **40**, 610 (2002).